Hindawi
Shock and Vibration
Volume 2023, Article ID 1737203, 13 pages
https://doi.org/10.1155/2023/1737203

Research Article

Seismic Behavior of Qinghai-Tibetan Railway Embankment in Permafrost Regions: A Case Study

Tuo Chen,[1,2] **Jianzhou Wang**,[1] **and Bo Wang**[1]

[1]*The State Key Laboratory for Geomechanics and Deep Underground Engineering, China University of Mining & Technology, Xuzhou 221116, China*
[2]*Key State Laboratory of Frozen Soil Engineering, Northwest Institute of Eco-Environment and Resources, CAS, Lanzhou 730000, China*

Correspondence should be addressed to Jianzhou Wang; wjzh@cumt.edu.cn

Received 5 May 2022; Revised 19 October 2022; Accepted 7 February 2023; Published 20 February 2023

Academic Editor: Ai Lan Che

The temperature is a critical factor that determines the unfrozen water content and ice content in the frozen soil. In view of mechanical properties of the frozen soil depend on the volume of components of the four-phase systems, thus the temperature has a significant impact on the mechanical behaviors and deformation properties. The thermal state of the embankment in permafrost regions has a significant seasonal difference, then the seismic performance of the embankment alters with the season. In addition, the seismic performance is highly influenced by the properties of the earthquake motion, especially the seismic intensity. Combining these factors, a numerical simulation was conducted in this study. In this study, taking a typical section of Qinghai-Tibet Railway as an example, a numerical case study on the seismic behavior of embankment was carried out using the dynamic explicit FEM code ABAQUS/Explicit. The El Centro excitation with different intensities was performed in numerical analysis and two distinct thermal states of the embankment in extreme cold and warm days were considered as well. The seismic behaviors of the embankment, including the acceleration responses, the strain response, and the displacement response, were studied effectively. This paper proposes approaches and methods to study the seismic failure mechanism of the infrastructures, and the results can serve as a scientific basis for resisting earthquakes and preventing disasters in cold regions.

1. Introduction

The Qinghai-Tibet Plateau (QTP) is the largest high-altitude permafrost region at low- and mid-latitudes in the world [1]. The permafrost area on the Qinghai-Tibet Plateau is estimated to be about $1.04 \times 10^6 \text{km}^2$ [2]. With the in-depth implementation of the western China development strategy and the construction of "Belt and Road," there is an increasing demand for cold region engineering in China. It is imperative to construct major national strategic projects in high-altitude permafrost regions. The Qinghai-Tibet Expressway, the Golmud—Lhasa oil product pipeline, the high voltage power transmission and transformation line, and other major construction projects will be constructed on the QTP. Furthermore, it needs to be recognized that the tectonic movement and crustal deformation are very strong and active faults are widely distributed. The QTP is located in the region with the most intensive deformation and high-level seismic activities. Seismologists are now suggesting the QTP has entered the third active seismic period since 1995 [3]. A sequence of large earthquakes occurred, including the Mani earthquake (Ms 7.9) on November 8, 1997; the Kunlunshan earthquake (Ms 8.1) on November 14, 2001; the Wenchuan earthquake (Ms 8.0) on May 12, 2008; the Yushu earthquake (Ms 7.1) on April 14, 2010; the Yutian earthquake (Ms 7.3) on February 12, 2014, and the Menyuan earthquake (Ms 6.9) on January 8, 2022, has attracted attention from engineers and researchers. These earthquakes produced surface ruptures with complicated structures and a great length, which had brought enormous damages to the transport infrastructures in the QTP area. Figure 1 illustrates the surface rupture zone in the permafrost area caused by the

Kunlunshan earthquake and the Menyuan earthquake, respectively. The potential earthquake risk has been a significant engineering challenge to the construction and maintenance of infrastructure in permafrost regions [4]. As a typical transport infrastructure, railway embankment damage, including rupture and deformation, may occur during an earthquake. Furthermore, the damage of the embankment was not observed in a typical earthquake. Thus the study of seismic response of linear engineering structures in permafrost regions, especially railway engineering, has become a key problem that needs to be solved as soon as possible.

Frozen soil is a kind of composite material composed of soil, unfrozen water, and ice. Compared with ordinary soil, the most obvious physical quantities are freezing temperature and unfrozen water content [5, 6]. Due to mechanical instability and temperature sensitivity, frozen soil can be categorized as "special" soil and its physical and mechanical properties may broadly differ across seasons [7]. As for the embankment engineering in cold regions, the interaction between frozen soil and climatic system directly affects the seismic dynamic response and failure characteristics. The seismic performance varies significantly in different seasons and regions, directly influencing the strategies of earthquake prevention and disaster mitigation. Thus, it is essential to study the seismic response and dynamic stability of the embankment in permafrost regions. The most direct research approach to studying the seismic behavior of structures is the shaking table test. In recent years, this method has been used wildly in embankment engineering [8–11]. However, there still have some shortcomings to this method, such as the huge cost and time-consuming, reduced scale model testing. Furthermore, it is very difficult to consider the effects of environmental factors on the seismic behavior of the embankment, such as the freezing and thawing process. With the rapid development of computer technology, the numerical analysis method has become an important and practical tool and provides an economical way to study the seismic behavior of embankments in permafrost regions. Wang et al. [12, 13] studied the earthquake dynamic stress characteristic and seismic displacement characteristic of the roadbed on permafrost site, and then proposed the stress intensity criteria of earthquake breakage. Esmaeili and Noghabi [14] developed a finite-element model to investigate the dynamic behavior of ballasted railway tracks subjected to earthquake motion. Chen et al. [15] discussed the impact of permafrost change on the seismic site response and then studied the dynamic response of the traditional embankment in permafrost regions. Li et al. [16, 17] investigated seasonal differences in seismic responses of an embankment on a sloping ground in permafrost regions. In addition, a thermo-dynamic coupled model for the crushed-rock embankment was proposed and a series of numerical computations were conducted. However, despite the fact that seismic responses of embankments in permafrost regions have been studied by many authors, few papers have been published on the seasonal differences in seismic responses of embankments in permafrost regions induced by an earthquake with different intensities.

In this work, based on a prototype of a typical traditional embankment at the Beiluhe section of the QTR, a full-scale simulation model is established to study the seismic behavior of the embankment under earthquake excitation. An actual seismic record (EI Centro earthquake, 1940) is selected as the input ground motion and different intensities were considered. Moreover, two distinct thermal states of the embankment on extreme cold and warm days are considered as well. The seismic behaviors of an embankment, including the acceleration responses, the strain response, and the displacement response, were studied effectively. The objective of this research is to obtain more details about the seismic behaviors of the embankment and to investigate the seismic damage evolution and failure process of embankment in permafrost regions.

2. Numerical Model and Basic Equations

2.1. Model of Railway Embankment. The Beiluhe segment, located in an arid climate region of QTP, belongs to the unfavorable and bad engineering geological section. The MAGT of this segment varies from −1.41 and −1.68°C. The freezing period of which is from September to the following April [18]. The active layer thaws in summer while freezes in winter, and the natural permafrost table of the segment is between −2 m and −3 m [19]. Moreover, the thick ice layer underground near the permafrost table is abundant, and the temporal and spatial variations in the thermal regime are observed in this segment. Whereas, different types of embankments have been constructed, such as traditional embankments, crushed-rock embankments, duct-ventilated embankments, and thermosiphon embankments.

Figure 2 illustrates the cross-section profile of a typical traditional embankment and the soil layer structure at the Beiluhe section K1137 + 700 of the QTR. The surface layer of the ground, defined as the active layer, is a gravelly sand layer. Beneath the active layer, there exists the frozen silty clay, also named as permafrost. The underlying permafrost contains the upper ice-poor permafrost with a thickness of 6 m and the lower ice-poor permafrost with a thickness of 22 m. According to the ground temperature measurement conducted by the State Key Laboratory of Frozen Soil Engineering, Chinese Academy of Science, the natural ground temperature variation and the distribution of mean annual ground temperature are defined; [20–22]. The natural permafrost table is approximately 2 m, and the temperature of the permafrost in this area is about −1.0°C.

Based on the prototype of the typical traditional embankment at the Beiluhe section, a full-scale numerical model of the embankment is established, as shown in Figure 3. The simulation is performed based on the plane strain assumption. In this study, the size of the mesh was controlled in order to guarantee the accuracy of dynamic analysis. The mesh size is limited by the shortest wavelength of the input seismic wave. To ensure the authenticity of wave propagation in the media, the maximum size of the element must be less than 1/10~1/8 of the minimum wavelength. In our simulation, the maximum mesh size is only 1 m × 1 m, and the accuracy of calculation meets the requirements.

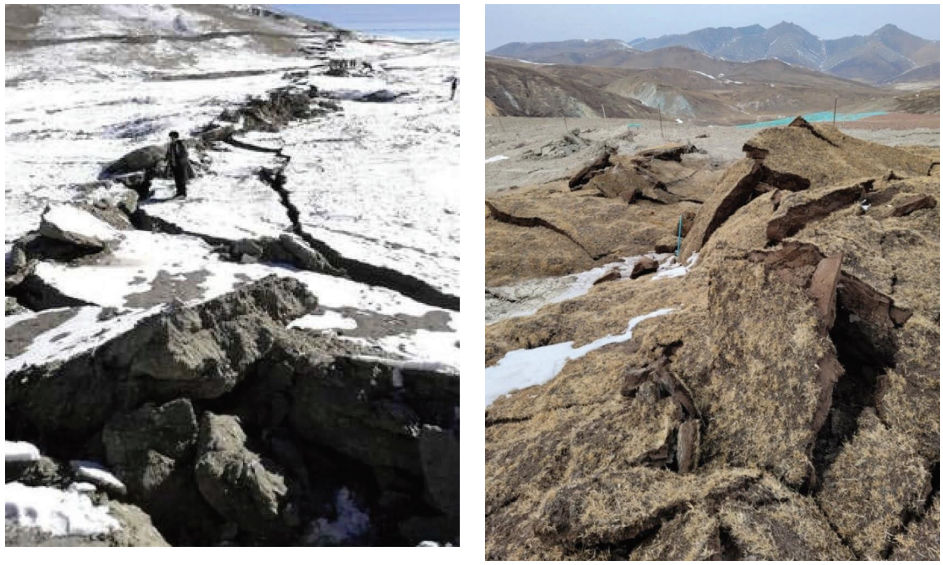

(a) (b)

Figure 1: Surface rupture zone in permafrost area caused by earthquakes: (a) Kunlunshan earthquake; (b) Menyuan earthquake.

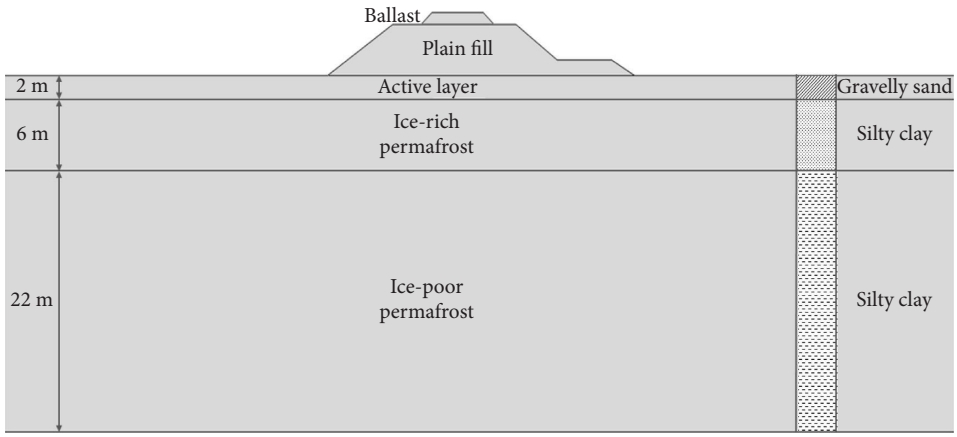

Figure 2: The cross-section profile and the soil layer structure of a typical traditional embankment.

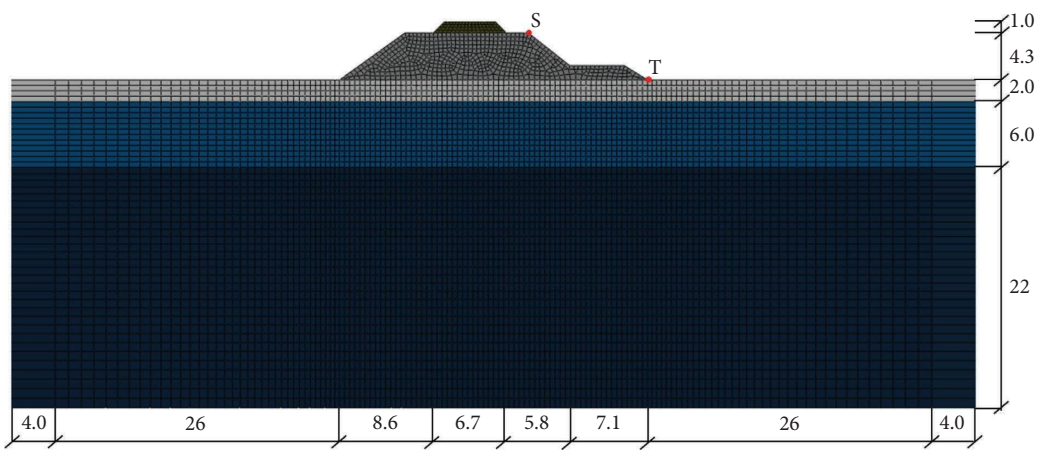

Figure 3: The full-scale numerical model of a typical traditional embankment (unit: m).

In the numerical model, two different boundary conditions are used, respectively. On the left and right sides of the numerical model, the free field method is taken to prevent wave reflection at the boundary of the embankment model. Moreover, the artificial boundary conditions are adopted at the bottom of the model where the horizontal direction is released and the artificial seismic waves are used as the input seismic motion for the numerical calculation.

2.2. Basic Equations. To study the dynamic behavior of the Qinghai-Tibet railway embankment under seismic loads, the nonlinear dynamic finite element analysis method is applied. The kinetic equation can be expressed as follows:

$$M \bullet \ddot{x}(t) + C \bullet \dot{x}(t) + K \bullet x(t) = P(t), \tag{1}$$

where M, C, and K are, respectively, the mass matrix, stiffness matrix, and damping matrix. $P(t)$ refers to the dynamic loading.

When the dynamic loading is small, the soil is in an elastic stage which adopts the linear elastic model, its stress-strain relation meets Hook's law. When the loading is getting greater, the elastoplastic properties of the soil need to be considered. As for any stress increment $d\{\sigma\}$, the total strain increment $d\{\varepsilon\}$ includes elastic strain increment $d\{\varepsilon^e\}$ and plastic strain increment $d\{\varepsilon^p\}$, which could be written as follows:

$$d\{\varepsilon\} = d\{\varepsilon^e\} + d\{\varepsilon^p\} = [D_T]^{-1} d\{\sigma\} + d\lambda \left\{\frac{\partial F}{\partial \sigma}\right\}, \tag{2}$$

where $[D_T]$ is the elastic matrix related to temperature and unfrozen water, the $d\lambda$ is the plastic coefficient, and F represents the plastic potential function.

In this paper, the Mohr–Coulomb elastic-plastic yield criterion is utilized to express the plastic potential function. This criterion assumes that soil failure occurs when shear stress in the plane of the material exceeds the value, which is linearly dependent on the normal stress to that plane [23, 24]. The Mohr–Coulomb criterion can be written as follows:

$$F = \frac{J_1}{3} \sin\varphi + \sqrt{J_2'} \left(\cos\theta - \frac{1}{\sqrt{3}} \sin\theta \sin\varphi \right) - C \cos\varphi = 0, \tag{3}$$

where J_1 is the first stress tensor invariant; J_2' denotes the second deviatoric stress tensor invariant, and θ is the Lode angle. C denotes the cohesive strength and φ denotes the internal friction angle, C and φ are related to the temperature.

3. Model Parameters and Input Seismic Motion

The freezing and thawing states are different at different times with the variation of the air temperature, which influences the soil water migrations in the embankment. The seismic behavior analysis of the embankment in the permafrost area is a very complicated problem when considering this impact. However, in order to simplify the study, two extreme situations including the warmest and coldest seasons are considered. In the warmest season, the roadbed filling and the active layer are supposed to be completely thawed. While in the coldest season, the roadbed filling and the active layer are fully frozen. The mudstone is always frozen all year round. The soil was regarded as an elastic-plastic material and the ballast was assumed to be a linear elastic material [25]. Then different soil mechanic parameters are endowed in different situations. The mechanical parameters of the numerical model are presented in Table 1, based on a series of triaxial tests [26–28]. The temperature in Table 1 is determined based on the ground temperature data at the Beiluhe section.

In this work, the El Centro earthquake wave (N-S direction) that occurred in 1940, is selected as seismic load in the numerical case study. Acceleration time history and fast Fourier transform (FFT) curves are presented in Figure 4. The maximum acceleration is 0.348 g and the predominant frequency is 1.47 Hz.

According to the seismic intensity zoning map in China, the QTP is located in areas with high seismic intensity above VII degrees. Thus in the numerical analysis, the acceleration amplitude of the input seismic motion is adjusted from 0.15 g to 0.4 g, which corresponds to different earthquake intensities (from intensity VII to intensity IX). The adjusted amplitudes and the amplification coefficients are shown in Table 2.

4. Numerical Simulation Results

In order to accurately capture the mechanical behavior of the embankment during the seismic loading, the acceleration response characteristics are investigated, as well as the dynamic strain and displacement response. Considering the dynamic stability of the embankment is largely concerned, then the characteristic point S on the embankment's shoulder and the characteristic point T at the toe of the embankment, are arranged in the model.

4.1. Acceleration Response Analysis. In this case study, the seismic input motion is in the horizontal direction and thus the horizontal acceleration response of the embankment in different seasons is investigated. The acceleration contour map of the embankment in warm and cold seasons, under the El Centro seismic motion, are depicted in Figures 5(a) and 5(b), respectively.

It can be well demonstrated that the rail embankment has an obvious amplification effect on the seismic wave, comparing the natural surface. The acceleration response of the embankment is greater in the warm season than in the cold season. Furthermore, the maximum acceleration appears at the top of the embankment in the cold season, while the acceleration at both embankment slopes is more significant in the warm season. The main reason for this phenomenon is the stiffness improvement of the embankment in cold seasons. The elastic modulus and strength of soil inside the embankment are distinctly enhanced. Consequently, the seismic acceleration responses of the

Table 1: Soil mechanics parameters at the survey area.

Lithology	Water content (%)	Temperature (°C)	Density (kN/m^3)	Elastic modulus (kPa)	Poisson ratio	Cohesion force (kPa)	Internal frictional angle
Ballast	—	5	20.0	2.00*E*5	0.30	—	—
Roadbed filling	26.3	2	19.0	6.10*E*4	0.31	30	23°
	26.3	−1	19.0	1.14*E*5	0.29	120	32°
Silty clay	20	0.5	18.0	2.80*E*4	0.35	150	22°
	20	−1	18.0	5.40*E*4	0.31	240	30°
Mudstone	15.2	−1	21.0	3.40*E*5	0.25	340	39°

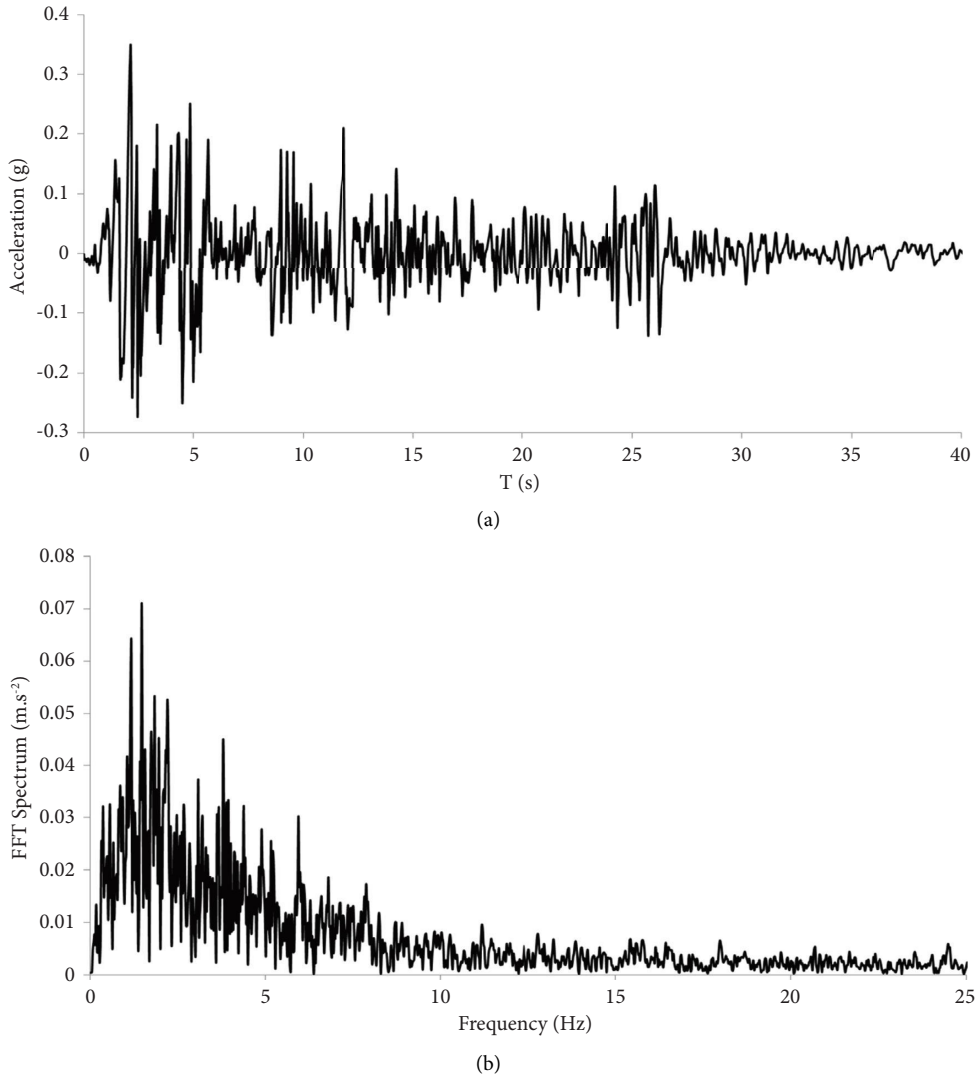

Figure 4: Acceleration time historie and FFT spectra of El Centro earthquake wave: (a) the acceleration time history; (b) the FFT spectra.

Table 2: Adjusted amplitudes and the amplification coefficients of the input seismic load.

Adjusted amplitude	0.15 g	0.2 g	0.25 g	0.3 g	0.348 g	0.4 g
Amplification coefficients	0.43	0.57	0.72	0.86	1.0	1.15
Seismic intensity	VII	VIII	VIII	VIII	VIII	IX

embankment are weakened, which is similar to the soil reinforcement effect.

The acceleration time history curve of the characteristic point S and point T is indicated in Figures 6(a) and 6(b), respectively. The maximum acceleration on the embankment's shoulder is 8.45 $m{\cdot}s^{-2}$ and 7.86 $m{\cdot}s^{-2}$ in the warm and cold seasons, respectively. In contrast, the maximum acceleration at the toe of the embankment is 5.08 $m{\cdot}s^{-2}$ and 4.65 $m{\cdot}s^{-2}$ in the warm and cold seasons, respectively. The acceleration amplitude becomes larger in the warm season and the amplification effect of the embankment's shoulder is more significant compared with the toe of the embankment.

In order to quantify the seismic response of the rail embankment, the maximum acceleration is characterized using the amplification coefficient, which is defined as the ratio of peak ground acceleration to input seismic acceleration. The variation of amplification coefficients with the input ground motion acceleration amplitude, of characteristic points S and T, are illustrated in Figure 7.

The results indicate that the acceleration amplification coefficient of railway embankment is significantly larger in warm seasons compared with cold seasons, and the acceleration amplification effect on the embankment's shoulder is more significant than the slope toe. Moreover, the

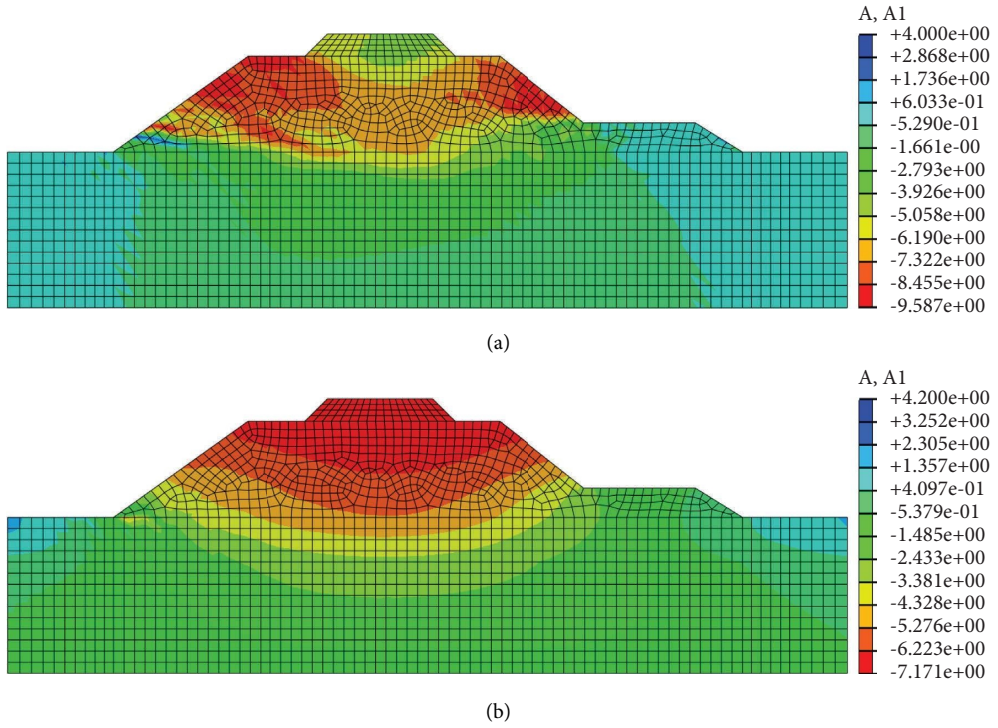

Figure 5: The Peak ground horizontal acceleration contour in different seasons: (a) horizontal acceleration contour map of the embankment in the warm season; (b) horizontal acceleration contour map of the embankment in the cold season.

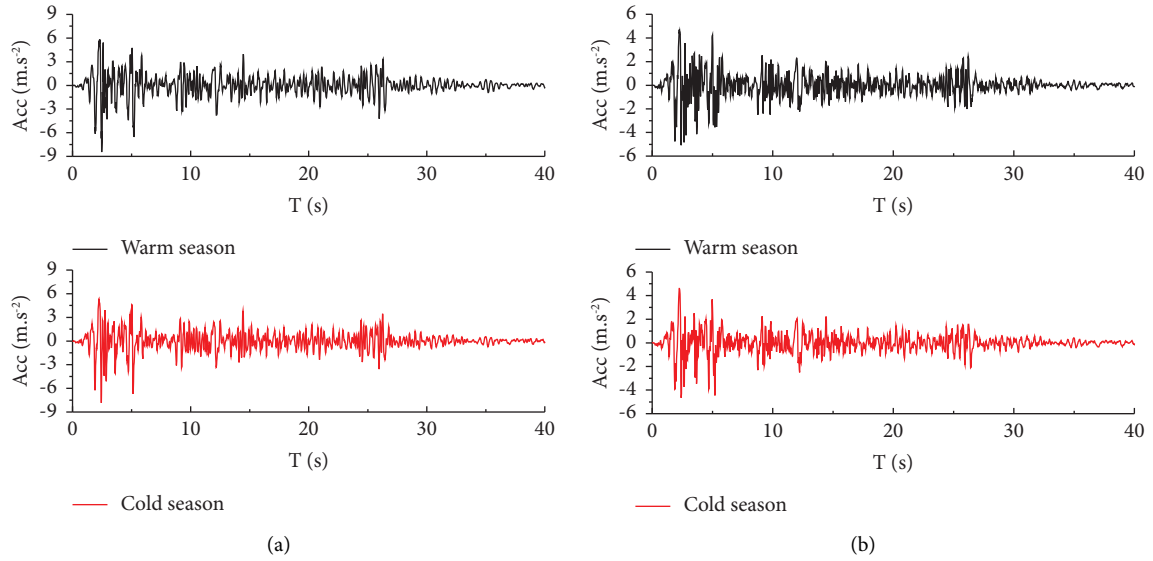

Figure 6: The acceleration time history curve of the characteristic point in different seasons: (a) characteristic point *S*; (b) characteristic point *T*.

acceleration amplification coefficient will decrease with the increase of input acceleration amplitude, exhibiting approximately linear characteristics. This tendency can be expressed using the following linear formula in slope-intercept form:

$$y = -kx + b. \tag{4}$$

In the formula mentioned above (equation (4)), the slope parameter k indicates the attenuation degree of acceleration,

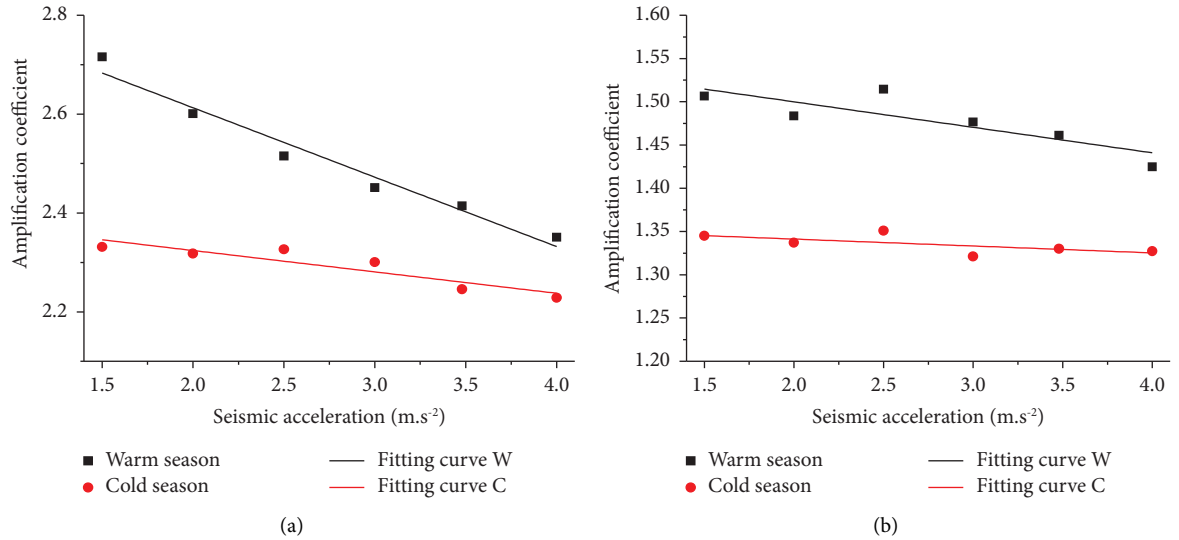

FIGURE 7: The variation of amplification coefficient with the input ground motion acceleration amplitude: (a) characteristic point *S*; (b) characteristic point *T*.

and the intercept parameter b shows the maximum amplification coefficient, as shown in Table 3.

4.2. Velocity Response Analysis. The velocity time history curve of the characteristic point *S* and point *T* is indicated in Figures 8(a) and 8(b), respectively. The maximum velocity on the embankment's shoulder is 0.84 m·s^{-1} and 0.67 m·s^{-1} in the warm and cold seasons, respectively. In contrast, the maximum acceleration at the toe of the embankment is 0.60 m·s^{-1} and 0.54 m·s^{-1} in the warm and cold seasons, respectively. The velocity response is greater in the warm season and the value is larger on the embankment's shoulder compared with the toe of the embankment.

Figure 9 illustrates the variation of the maximum velocity magnitude with the input ground motion acceleration amplitude. The maximum velocity magnitude increases with the increase of input acceleration amplitude. Moreover, the velocity difference ΔV between the point *S* and point *T* increases with the increasing input acceleration, and this value in the warm season ΔV_w is greater than in the cold season ΔV_c. It is indicated that the embankment is prone to cracking or deformation in the warm season.

4.3. Displacement Response Analysis. Figure 10 illustrates the displacement time history on the embankment's shoulder in a horizontal direction. This displacement is the relative value between point *S* and point *T*. The displacement changes nonlinearly with the duration time of the earthquake, presenting a maximum value at the peak acceleration time. The maximum displacement on the embankment's shoulder is 7.44 cm and 6.74 cm in the warm and cold seasons, respectively.

Figure 11 illustrates the distribution of the maximum relative displacement with the input ground motion acceleration amplitude in different seasons. As observed in Figure 10, the horizontal displacement on the embankment's shoulder is larger in the warm season than in the cold season. The displacement increases with the increase of input ground motion acceleration amplitude, and the variation tendency is approximately linear. The maximum displacement on the embankment's shoulder can reach up to 9 cm under the action of 0.4 g seismic excitation in the warm season, while this value is only 2.6 cm under the action of 0.2 g seismic excitation in the cold season. It can be considered that cracks or even collapse will occur when the input peak acceleration reaches a certain value.

4.4. Strain Response Analysis. Figure 12 illustrates the maximum plastic strain of the embankment under the seismic motion with different peak accelerations, in different seasons. It is concluded from the results that the plastic zone gradually appears in the embankment when the seismic intensity reaches a certain value. The plastic zone starts to develop at the slope toe of the embankment, and there exists a continuous extension of the plastic zone with the increase of the seismic intensity. Moreover, on the left side of the embankment, where there is no pavement, the plastic strain exponent is larger and the plastic deformation was significantly higher.

Subsequently, the variation of the maximum plastic strain magnitude in the railway embankment with the input ground motion acceleration amplitude is illustrated in Figure 13. With the increase of input acceleration amplitude, the maximum plastic strain magnitude increase, and this trend is more significant in warm seasons. In a warm season, there is no plastic zone generated in the embankment until the input acceleration amplitude reaches 2.0 m·s^{-2}. The plastic strain magnitude ranges from 4.43 $E-3$ to 2.92 $E-2$, and the corresponding acceleration amplitude is within the range from 2.0 to 4.0 m·s^{-2}. In a cold season, the plastic will appear when the input acceleration amplitude reaches 2.5 m·s^{-2}, and the plastic strain magnitude varies from

Table 3: The value of slope and intercept parameter.

Characteristic point	The location	Characteristic time	Slope-intercept parameters	
			k	b
S	Embankment's shoulder	Warm season	0.14	2.89
	Embankment's shoulder	Cold season	0.04	2.41
T	Embankment slope toe	Warm season	0.02	1.56
	Embankment slope toe	Cold season	0.007	1.36

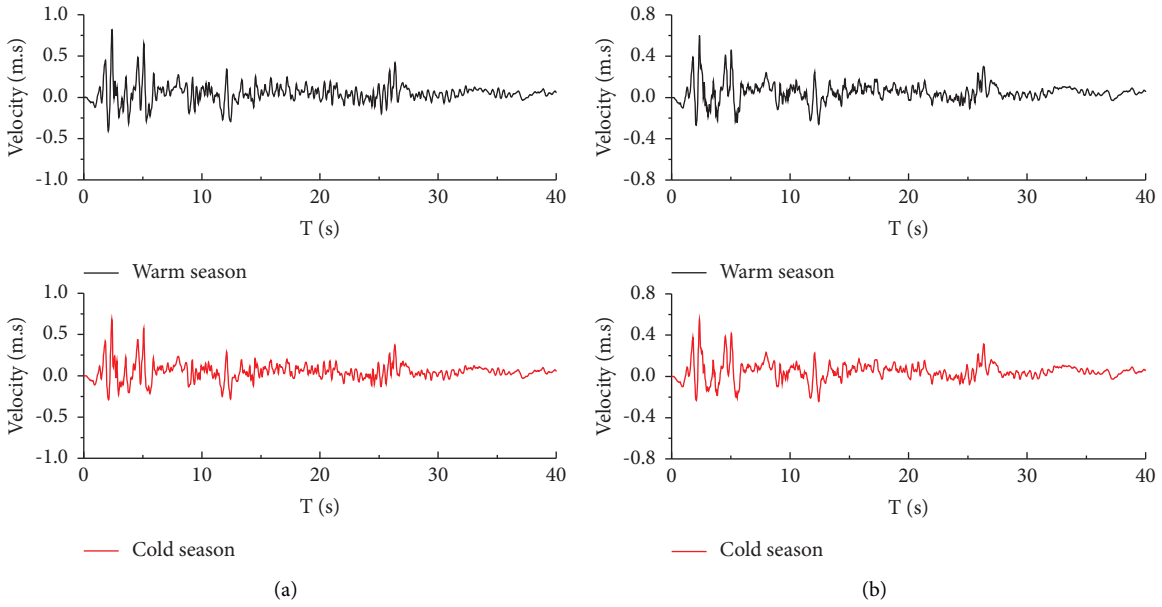

Figure 8: The velocity time history curve of the characteristic point in different seasons: (a) characteristic point S; (b) characteristic point T.

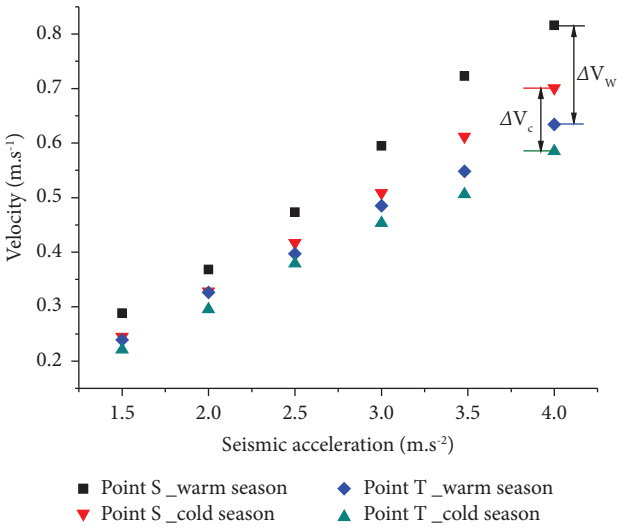

Figure 9: The variation of maximum velocity with the input ground motion acceleration amplitude.

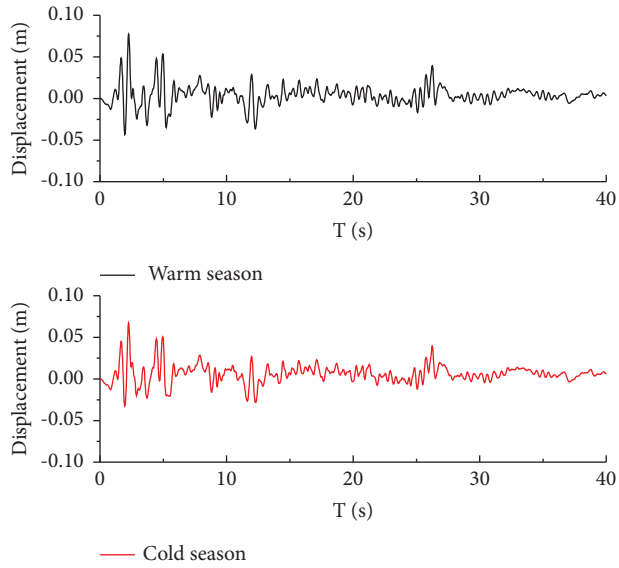

Figure 10: The displacement time history on the embankment's shoulder.

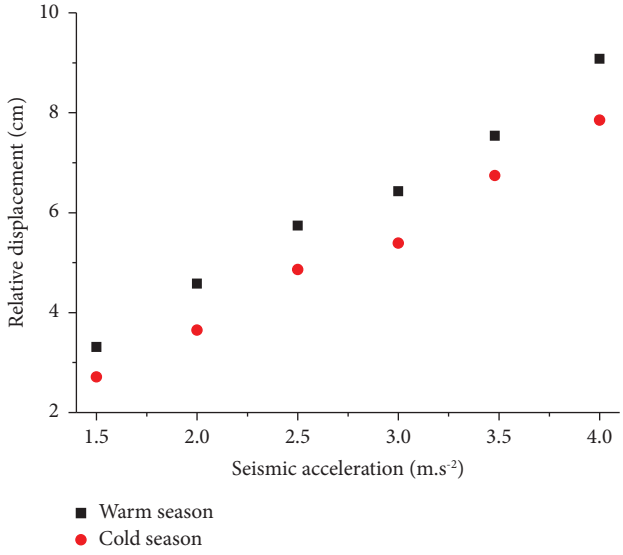

Figure 11: The distribution of the maximum relative displacement.

2.19 $E-3$ to 6.17 $E-3$ when the input acceleration amplitude change from 2.5 to 4.0 m·s^{-2}.

5. Discussion

It has now been confirmed that the seismic response of the embankment structure in permafrost regions is a very complicated water-heat-dynamic coupled problem. There is a real difficulty in the ability to simulate soil hydrothermal transport processes and the deformation-damage-failure process, especially under earthquake excitation. Because of this, very few theoretical and practical results available up to now. As a preliminary study, the numerical simulation in this paper still has some deficiencies. But despite this, the results of our study are consistent with the findings of previous research. Furthermore, our study has revealed some other interesting findings. It is observed that the location of the maximum plastic strain that occurred seems not to coincide with the peak acceleration locations. Because the plastic strain is a parameter to quantify the damage, which reflects the differences or the relationship between the stress and strength. While the acceleration response characteristic is mainly related to the soil layer stiffness.

In this paper, starting from the variation of the dynamic response characteristics, we try to make a quantitative risk analysis of the embankment in permafrost regions. Through our research work, it is found that the vulnerability evaluation of the embankment becomes possible when associated with the variation of the plastic strain.

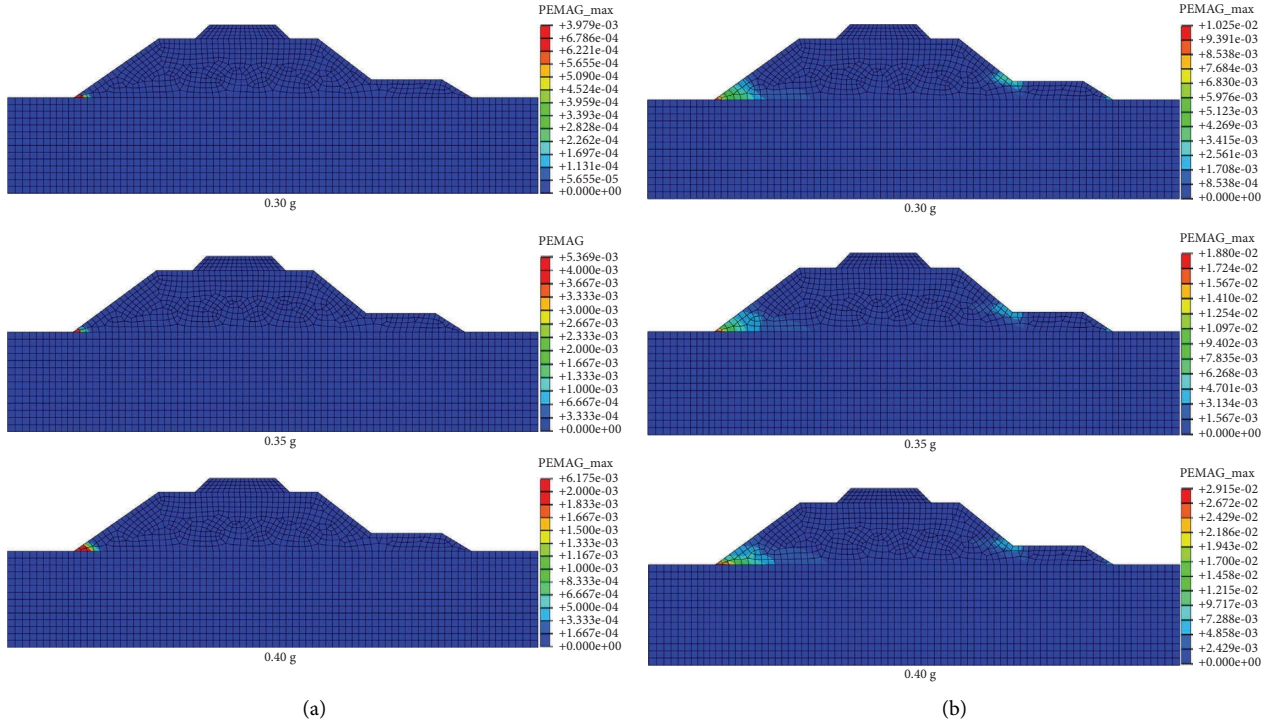

Figure 12: The maximum plastic strain of the embankment under the seismic motion: (a) in the cold season; (b) in the warm season.

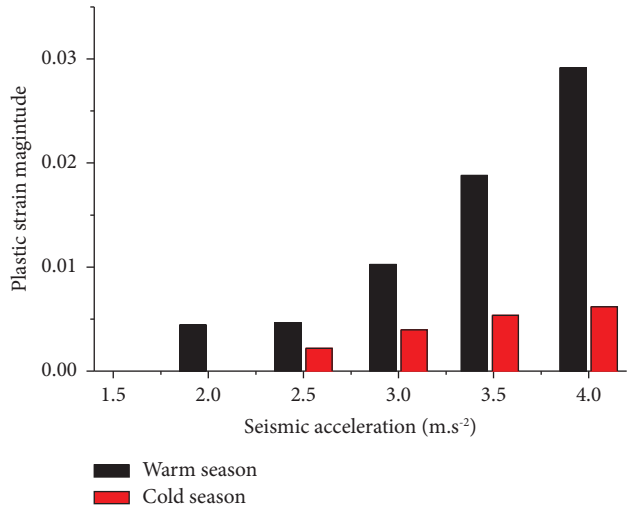

Figure 13: The variation of maximum plastic strain with the input ground motion acceleration amplitude.

6. Conclusions

In this work, based on a prototype of a typical traditional embankment at the Beiluhe section of the QTR, a full-scale simulation model is established and a numerical case study on the seismic behavior of embankment is performed. Two different thermal states of the embankment in extreme cold and warm days are considered, and the influence of seismic intensity on the dynamic response is discussed. The following conclusions can be drawn from the results of this study:

(1) The dynamic response at different positions of the embankment varies greatly in different seasons. The maximum acceleration appears at the top of the embankment in the cold season, while the acceleration at both embankment slopes is more significant in the warm season.

(2) From the acceleration, velocity, and displacement analysis, it can be concluded that cracks or even collapses will occur when the input peak acceleration reaches a certain value. The embankment is prone to collapse or damage in the warm season.

(3) The acceleration amplification coefficient will decrease with the increase of input acceleration amplitude, exhibiting approximately linear characteristics. The displacement increases with the increase of input ground motion acceleration amplitude, and the variation tendency is approximately linear.

(4) With the increase of input acceleration amplitude, the maximum plastic strain magnitude increase, and this trend is more significant in warm seasons. In a warm season, there is no plastic zone generated in the embankment until the input acceleration amplitude reaches 2.0 $m \cdot s^{-2}$. In a cold season, the plastic will appear when the input acceleration amplitude reaches 2.5 $m \cdot s^{-2}$.

Data Availability

All data included in this study are available from the corresponding author upon request.

Conflicts of Interest

The authors declare that they have no conflicts of interest.

Acknowledgments

This study is financially supported by the National Natural Science Foundation of China (grant nos. 41701058 and 51874286), the Open Fund of State Key Laboratory of Frozen Soil Engineering (grant no. SKLFSE201606). The authors would like to express their sincere thanks to the anonymous reviewers for their valuable suggestions and constructive comments which greatly improved the presentation of this paper.

References

[1] X. Li, Q. Wu, R. Li et al., "Characteristic, changes and impacts of permafrost on Qinghai-Tibet Plateau," *Chinese Science Bulletin*, vol. 64, no. 27, pp. 2783–2795, 2019.

[2] J. Ni, T. Wu, X. Zhu et al., "Simulation of the present and future projection of permafrost on the Qinghai-Tibet Plateau with statistical and machine learning models," *Journal of Geophysical Research: Atmospheres*, vol. 126, no. 2, Article ID e2020JD033402, 2021.

[3] Q. D. Deng, S. P. Cheng, J. Ma, and P. Du, "Seismic activities and earthquake potential in the Tibetan plateau," *Chinese Journal of Geophysics*, vol. 57, no. 7, pp. 2025–2042, 2014.

[4] A. M. Lin, B. H. Fu, J. M. Guo et al., "Coseismic strike-slip and rupture length produced by the 2001 Ms 8.1 Central Kunlun Earthquake," *Science*, vol. 296, no. 5575, pp. 2015–2017, 2002.

[5] Z. W. Wu and Y. Z. Liu, *Frozen Subsoil and Engineering*, Ocean Press, Lancing, England, 2005.

[6] F. J. Niu, J. M. Zhang, and J. Z. Zhang, "Engineering geological characteristics and evaluations of permafrost in Beiluhe testing field of Qinghai-Tibetan Railway," *Journal of Glaciology and Geocryology*, vol. 24, no. 3, pp. 264–269, 2002.

[7] L. U. Arenson and S. M. Springman, "Mathematical descriptions for the behaviour of ice-rich frozen soils at temperatures close to 0 °C," *Canadian Geotechnical Journal*, vol. 42, no. 2, pp. 431–442, 2005.

[8] J. B. Li, H. R. Zhang, and Z. Q. Li, "Large scale shaking table test study of dynamic response and dynamic failure of subgrade," *Chinese Journal of Rock Mechanics and Engineering*, vol. 30, no. S2, pp. 3746–3754, 2011.

[9] Y. L. Lin, "Deformation behavior of reinforced embankment slopes under seismic excitation," *Disaster Advances*, vol. 6, no. 7, pp. 12–19, 2013.

[10] C. W. Yang, X. H. Tong, and D. Wang, "Shaking table test of dynamic response law of subgrade with ballast track under earthquake," *Rock and Soil Mechanics*, vol. 41, no. 7, pp. 2215–2223, 2020.

[11] W. Z. Chen, Y. Liu, and H. Y. Chen, "Shaking table test on slope subgrade reinforced by boredpiles of Sichuan-Tibet railway," *Chinese Journal of Rock Mechanics and Engineering*, vol. 39, no. 12, pp. 2540–2556, 2020.

[12] L. X. Wang, X. Z. Ling, and X. Y. Xu, "Study on earthquake dynamic stress characteristic of roadbed on permafrost site," *Earthquake Engineering and Engineering Vibration*, vol. 24, no. 1, pp. 117–121, 2004.

[13] L. X. Wang and X. Z. Ling, "Study on differentiate criteria of earthquake breakage of frozen roadbed," *Chinese Journal of Rock Mechanics and Engineering*, vol. 24, no. 4, pp. 638–642, 2005.

[14] M. Esmaeili and H. H. Noghabi, "Investigating seismic behavior of ballasted railway track in earthquake excitation using finite-element model in three-dimensional space," *Journal of Transportation Engineering*, vol. 139, no. 7, pp. 697–708, 2013.

[15] T. Chen, W. Ma, and G. Q. Zhou, "Numerical analysis of ground motion characteristics in permafrost regions along the Qinghai-Tibet Railway," *Cold Regions Science and Technology*, vol. 148, pp. 88–95, 2018.

[16] S. Y. Li, Y. M. Lai, M. Y. Zhang, and W. Yu, "Seasonal differences in seismic responses of embankment on a sloping ground in permafrost regions," *Soil Dynamics and Earthquake Engineering*, vol. 76, no. 1, pp. 122–135, 2015.

[17] S. Y. Li, M. Y. Zhang, W. S. Pei, Y. Lai, and W. Yu, "Thermo-seismic characteristics of a crushed-rock interlayer embankment on a permafrost slope," *Cold Regions Science and Technology*, vol. 151, pp. 249–259, 2018.

[18] Z. Z. Sun, W. Ma, and D. Q. Li, "Ground temperature characteristics of block stone embankment characteristics of block stone embankment and traditional embankment at Beiluhe along Qinghai-Tibet Railway," *Chinese Journal of Geotechnical Engineering*, vol. 30, no. 2, pp. 303–308, 2008.

[19] M. L. Zhang, Z. Wen, and K. Xue, "The effects of precipitation on thermal - moisture dynamics of active layer at Beiluhe permafrost region," *Journal of Arid Land Resources & Environment*, vol. 30, no. 4, pp. 159–164, 2016.

[20] W. Ma, C. H. Shi, Q. B. Wu, L. X. Zhang, and Z. J. Wu, "Monitoring study on technology of the cooling roadbed in permafrost region of Qinghai–Tibet plateau," *Cold Regions Science and Technology*, vol. 44, no. 1, pp. 1–11, 2006.

[21] W. Ma, Y. H. Mu, Q. B. Wu, Z. Z. Sun, and Y. Z. Liu, "Characteristics and mechanisms of embankment deformation along the Qinghai–Tibet Railway in permafrost regions," *Cold Regions Science and Technology*, vol. 67, no. 3, pp. 178–186, 2011.

[22] Y. H. Mu, W. Ma, Q. B. Wu, Z. Z. Sun, Y. Z. Liu, and G. Qu, "Thermal regime of conventional embankments along the Qinghai–Tibet Railway in permafrost regions," *Cold Regions Science and Technology*, vol. 70, no. 1, pp. 123–131, 2012.

[23] M. Taiebat, H. Shahir, and A. Pak, "Study of pore pressure variation during liquefaction using two constitutive models for sand," *Soil Dynamics and Earthquake Engineering*, vol. 24, pp. 551–564, 2007.

[24] R. Uzuoka, N. Sento, M. Kazama, F. Zhang, A. Yashima, and F. Oka, "Three-dimensional numerical simulation of earthquake damage to group-piles in a liquefied ground," *Soil Dynamics and Earthquake Engineering*, vol. 27, no. 5, pp. 395–413, 2007.

[25] A. L. Che, I. Takahiro, and X. R. Ge, "Dynamic behaviors of subway structure subjected to strong earthquake motions using shaking table tests and dynamic analyses," *Rock and Soil Mechanics*, vol. 27, no. 8, pp. 1293–1298, 2006.

[26] S. P. Zhao, Y. L. Zhu, and P. He, "Testing study on dynamic mechanics parameters of frozen soil," *Chinese Journal of Rock Mechanics and Engineering*, vol. 22, no. 2, pp. 2677–2681, 2003.

[27] Y. M. Lai, Y. Zhang, S. J. Zhang, and L. Jin, "Experimental study of strength of frozen sandy soil under different water contents and temperatures," *Rock and Soil Mechanics*, vol. 30, no. 12, pp. 3665–3670, 2008.

[28] H. Du, W. Ma, S. Zhang, Z. Zhou, and E. Liu, "Strength properties of ice-rich frozen silty sands under uniaxial compression for a wide range of strain rates and moisture contents," *Cold Regions Science and Technology*, vol. 123, pp. 107–113, 2016.